Available online at www.sciencedirect.com
ScienceDirect
Journal of Power Sources 158 (2006) 1202–1208
JOURNAL OF POWER SOURCES
www.elsevier.com/locate/jpowsour

Synthesis and characterization of $Nd_{0.6}Sr_{0.4}Co_{1-y}Mn_yO_{3-\delta}$ ($0 \le y \le 1.0$) cathodes for intermediate temperature solid oxide fuel cells

K.T. Lee, A. Manthiram *

Materials Science and Engineering Program, University of Texas at Austin, Austin, TX 78712, USA

Received 19 September 2005; received in revised form 30 September 2005; accepted 3 October 2005
Available online 28 November 2005

Abstract

$Nd_{0.6}Sr_{0.4}Co_{1-y}Mn_yO_{3-\delta}$ ($0 \le y \le 1.0$) oxides have been investigated as cathode materials for intermediate temperature solid oxide fuel cells (SOFC). The samples form a single-phase solid solution with an orthorhombic perovskite structure and the lattice parameters and volume increase with increasing Mn content y. The degree of oxygen loss at high temperatures and the thermal expansion coefficient (TEC) decrease with increasing y due to a stronger Mn–O bond. The electrical conductivity decreases with y and the system exhibits a metal to semiconductor transition at around $y = 0.2$. The electrocatalytic activity and power density measured with single cell SOFC decrease with increasing y due to a decrease in oxygen exchange and mobility as well as charge transfer kinetics, arising from a decrease in the oxide ion vacancy concentration and electrical conductivity.

Keywords: Solid oxide fuel cells; Cathode materials; Electrical conductivity; Thermal expansion; Electrochemical performance

1. Introduction

Solid oxide fuel cells (SOFC) offer an important advantage of using hydrocarbon fuels directly without requiring external reforming to produce hydrogen compared to the proton exchange membrane fuel cells (PEMFC). They also employ less expensive ceramic oxide electrocatalysts without requiring the expensive and scarcely available platinum-based electrocatalysts. However, the usual operating temperature of around 1000 °C with the zirconia-based electrolytes leads to a limited choice of interconnect and cathode materials, thermal expansion mismatch, and chemical reactivity among the components [1,2]. These difficulties have generated enormous interest in lowering the operating temperature to an intermediate range of 500–800 °C. However, the major issue with the intermediate temperature SOFC is the decrease in catalytic activity of the cathode for the oxygen reduction reaction [3].

Recently, the Sr-doped lanthanum cobaltates ($Ln_{1-x}Sr_xCoO_{3-\delta}$) have been intensively investigated as cathode materials for intermediate temperature SOFC because of their high electronic and oxide ion conductivities [4–6]. $La_{1-x}Sr_xCoO_{3-\delta}$, however, exhibits a large thermal expansion coefficient (TEC). A replacement of La by smaller lanthanides could lower the TEC due to the decrease in the ionicity of the Ln–O bond [7]. Accordingly, other Sr-doped lanthanide cobaltates $Ln_{1-x}Sr_xCoO_{3-\delta}$ (Ln = Pr, Nd, Sm, and Gd) have been investigated as cathode materials for intermediate temperature SOFC [8–13].

We showed recently that the $x = 0.4$ composition in the system $Nd_{1-x}Sr_xCoO_{3-\delta}$ shows the highest catalytic activity without encountering any interfacial reaction with the electrolyte [14]. Although the catalytic activity observed at the intermediate temperatures is satisfactory, the TEC of $Nd_{0.6}Sr_{0.4}CoO_{3-\delta}$ is still high. With an aim to lower the TEC, we focus here on the substitution of Mn for Co and a characterization of the $Nd_{0.6}Sr_{0.4}Co_{1-y}Mn_yO_{3-\delta}$ ($0 \le y \le 1.0$) cathodes. The effect of Mn content on the crystal chemistry, thermal expansion, electrical conductivity and electrochemical performance in single cell SOFC is presented.

2. Experimental

The $Nd_{0.6}Sr_{0.4}Co_{1-y}Mn_yO_{3-\delta}$ ($0 \le y \le 1.0$) compositions were synthesized by firing required amounts of Nd_2O_3, $SrCO_3$, Co_3O_4 and Mn_2O_3 in air at 900 °C for 12 h, followed by grinding, pressing into pellets and sintering at 1300 °C for 24 h. The sintering at 1300 °C was repeated after regrinding

* Corresponding author. Tel.: +1 512 471 1791; fax: +1 512 471 7681.
E-mail address: rmanth@mail.utexas.edu (A. Manthiram).

0378-7753/$ – see front matter © 2005 Elsevier B.V. All rights reserved.
doi:10.1016/j.jpowsour.2005.10.021

and repelletizing to improve the product homogeneity. The $La_{0.8}Sr_{0.2}Ga_{0.8}Mg_{0.2}O_{2.8}$ (LSGM) electrolyte was prepared by firing required amounts of La_2O_3, $SrCO_3$, Ga_2O_3 and MgO at 1100 °C for 5 h, followed by pelletizing and sintering at 1500 °C for 10 h. NiO–$Ce_{0.9}Gd_{0.1}O_{1.95}$ (GDC) cermet (Ni:GDC = 70:30 vol%) anode was synthesized by the glycine–nitrate combustion method [15].

The products were characterized by X-ray diffraction and the lattice parameters were obtained by analyzing the X-ray diffraction data with the Rietveld method. BET surface area was measured by a Quantachrom Autosorb-1 surface area and pore size analyzer. Thermogravimetric analysis (TGA) and thermal expansion data were obtained with a Perkin-Elmer Series 7 thermal analysis system. TGA experiments were carried out from room temperature to 1000 °C in air with a heating rate of 2 °C min^{-1} and a cooling rate of 10 °C min^{-1}. The TECs of sintered samples were measured from room temperature to 700 °C with a heating/cooling rate of 5 °C min^{-1}. The electrical conductivity was measured by a four-probe dc method in the temperature range of 200–900 °C. All the samples used for conductivity and thermal expansion measurements had densities of >95% of theoretical values.

Electrochemical performance (*I–V*) measurements were carried out with single cells consisting of the $Nd_{0.6}Sr_{0.4}Co_{1-y}Mn_yO_{3-\delta}$ cathode, LSGM electrolyte and NiO–GDC cermet anode at 800 °C using a three electrode configuration, which allowed the separation and monitoring of cathode overpotentials during cell operation. Pt paste was used as the reference electrode on the cathode side. Fig. 1 shows the schematic configuration of the test cell. The $Nd_{0.6}Sr_{0.4}Co_{1-y}Mn_yO_{3-\delta}$ cathodes and NiO–GDC cermet anode were prepared by screen printing onto 1.0 mm thick LSGM electrolyte pellet, followed by firing for 3 h at 1100 °C for the cathode and 1200 °C for the anode. The geometrical area of the electrode was 0.25 cm^2. Humidified H_2 (~3% H_2O at 30 °C) and air were supplied as fuel and oxidant, respectively, at a rate of 100 cm^3 min^{-1}. AC impedance measurements were carried out with a potentiostat using a three electrode configuration in air. The test cell geometry and configuration were same as that used for the single cell performance test. Pt paste was used as both the counter and reference electrodes. The applied frequency was in the range of 0.5 mHz to 1 MHz with a voltage amplitude of 10 mV.

3. Results and discussion

The X-ray diffraction patterns of the $Nd_{0.6}Sr_{0.4}Co_{1-y}Mn_yO_{3-\delta}$ samples shown in Fig. 2 indicate that a single-phase solid solution is formed for the entire range of $0 \le y \le 1.0$. The patterns could be indexed on the basis of an orthorhombic perovskite ($GdFeO_3$ type) structure, and the lattice parameters and average crystallite size values are summarized in Table 1 along with the BET surface area. The data indicate that the lattice parameters and the lattice volume increase with increasing Mn content y due to the replacement of the smaller Co^{3+} ($r = 0.545$ Å) ions by the larger Mn^{3+} ($r = 0.645$ Å) ions [16]. This trend is similar to that reported previously by Phillipps et al. [17] for the analogous $Gd_{1-x}A_xCo_{1-y}Mn_yO_3$ (A = Sr and Ca) system.

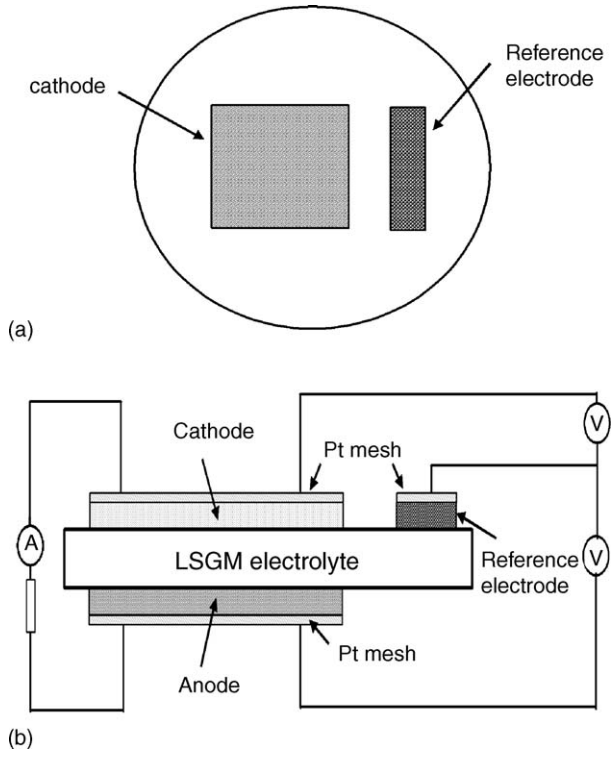

Fig. 1. Schematic configuration of the test single cell: (a) top view and (b) cross-sectional view.

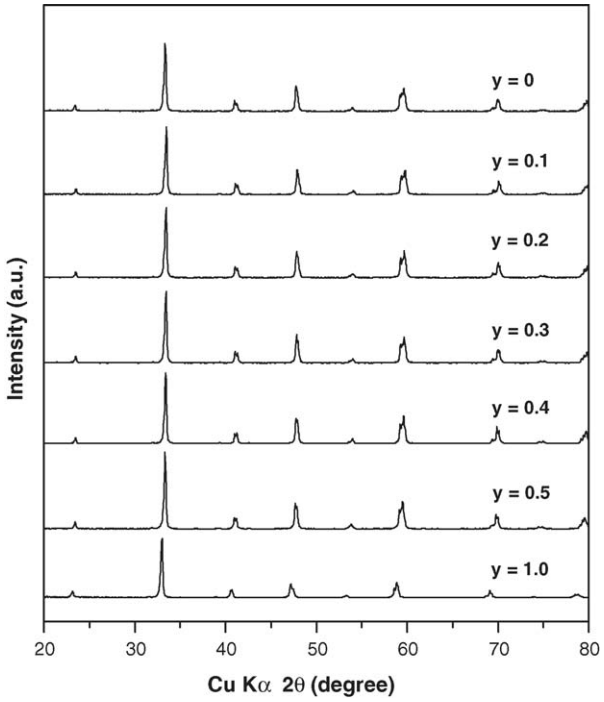

Fig. 2. X-ray powder diffraction patterns of $Nd_{0.6}Sr_{0.4}Co_{1-y}Mn_yO_{3-\delta}$ sintered at 1300 °C for 24 h.

Table 1
Crystal chemistry data, BET surface area and average crystallite size of $Nd_{0.6}Sr_{0.4}Co_{1-y}Mn_yO_{3-\delta}$

y	a (Å)	b (Å)	c (Å)	Lattice volume (Å^3)	BET surface area (m^2 g^{-1})	Average crystallite size[a] (Å)
0	5.3626(5)	5.4111(4)	7.5859(8)	220.1	3.98	478
0.1	5.3632(4)	5.4127(4)	7.5872(6)	220.3	4.25	455
0.2	5.3677(4)	5.4163(4)	7.5922(6)	220.7	3.11	523
0.3	5.3691(4)	5.4169(4)	7.5955(6)	220.9	4.12	461
0.4	5.3757(4)	5.4219(3)	7.6042(5)	221.6	3.55	511
0.5	5.3839(4)	5.4287(3)	7.6139(5)	222.5	3.81	494
1.0	5.4310(5)	5.4656(4)	7.6641(6)	227.5	3.02	527

[a] The average crystallite size was estimated from the line broadening of the XRD peaks.

TGA plots of the samples are shown in Fig. 3 for various y values. The samples exhibited good reversibility during the heating–cooling cycles in TGA, indicating that the observed weight loss during heating is due to the loss of oxygen from the lattice. The degree of oxygen loss decreases with increasing Mn content similar to that found before by us with Fe doping in $Nd_{0.6}Sr_{0.4}Co_{1-y}Fe_yO_{3-\delta}$ [18], suggesting a stronger binding of the oxygen to the lattice with increasing Mn content. While the end member $Nd_{0.6}Sr_{0.4}CoO_{3-\delta}$ begins to exhibit weight loss at temperatures as low as 400 °C, the end member $Nd_{0.6}Sr_{0.4}MnO_3$ does not exhibit any detectable weight loss to temperatures as high as 1000 °C. The observation is consistent with the suggestion of Steele [19] that perovskite oxides with Fe^{3+} and Mn^{3+} ions are thermally more stable than those with Co^{3+} ions. Moreover, the variations of oxygen content $(3-\delta)$ with pO_2 exhibit a plateau at $\delta = 0.5x$ for $La_{1-x}Sr_xMnO_{3-\delta}$ over a wide range of pO_2, while the $La_{1-x}Sr_xCoO_{3-\delta}$ system shows no such plateaus [20,21]. This implies a greater tendency for oxygen non-stoichiometry in the case of cobaltates compared to the manganates.

The thermal expansion behaviors of $Nd_{0.6}Sr_{0.4}Co_{1-y}Mn_yO_{3-\delta}$ at 50–700 °C in air are shown in Fig. 4a. The non-linear thermal expansion behavior could be fitted with a fourth polynomial regression [22,23]. The average TEC values obtained by the fitting are plotted as a function of Mn content y in Fig. 4b. The TEC value decreases with increasing Mn content similar to that

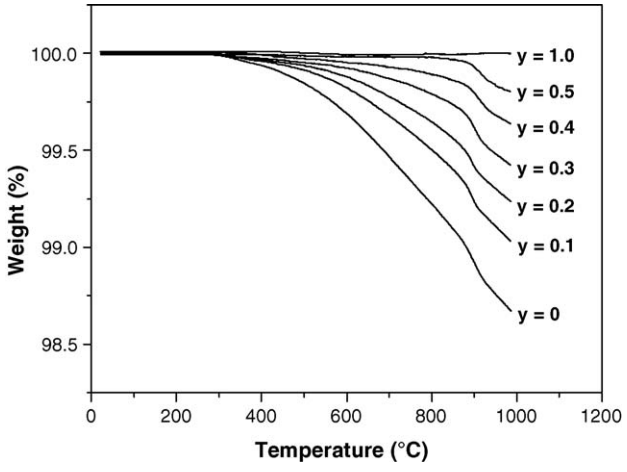

Fig. 3. TGA plots of $Nd_{0.6}Sr_{0.4}Co_{1-y}Mn_yO_{3-\delta}$ recorded in air with a heating rate of 2 °C min^{-1}.

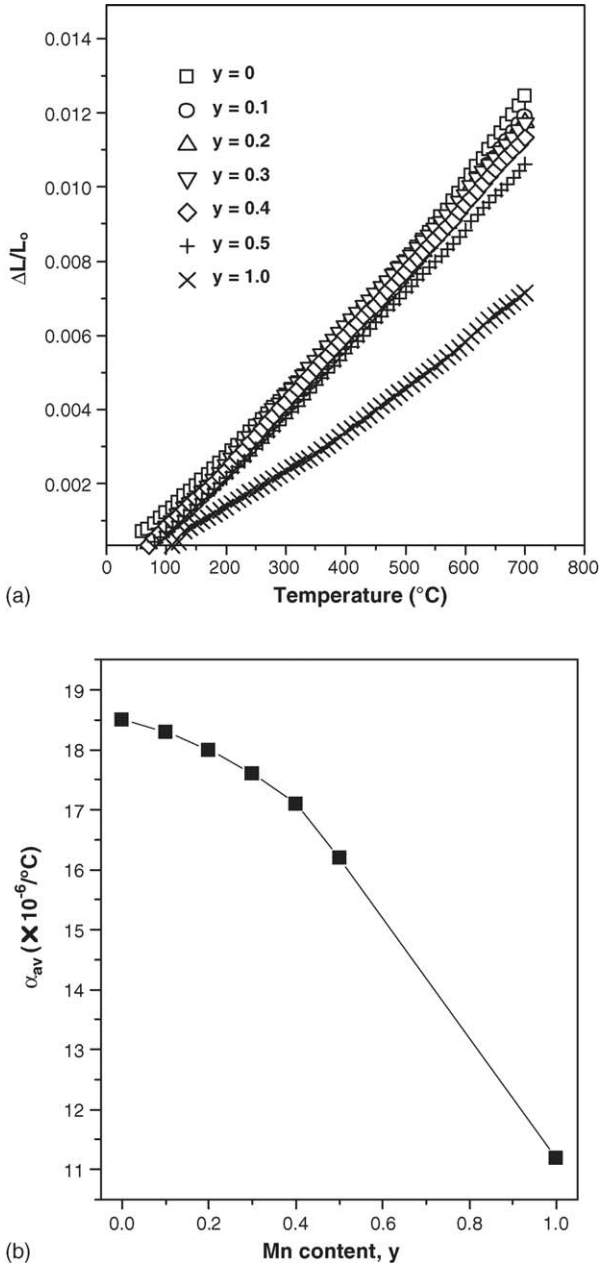

Fig. 4. Thermal expansion behaviors of $Nd_{0.6}Sr_{0.4}Co_{1-y}Mn_yO_{3-\delta}$ in air: (a) thermal expansion ($\Delta L/L_0$) curves as a function of temperature and (b) variation of the average thermal expansion coefficients (α_{AV}) with Mn content y in the temperature range of 50–700 °C.

found with Fe doping [18]. A similar trend has been observed for the analogous $Gd_{1-x}A_xCo_{1-y}Mn_yO_3$ (A = Sr and Ca) system before [17]. The larger TEC for the cobaltates can be attributed to the following two factors: (i) electronic transition from the low spin Co^{III} state $\left(t_{2g}^6e_g^0\right)$ to the high spin Co^{3+} state $\left(t_{2g}^4e_g^2\right)$ that is accompanied by an increase in ionic radius from 0.545 Å (low spin) to 0.61 Å (high spin) [24] and (ii) formation of oxygen vacancies that results in a decrease in the formal oxidation state of the transition metal ion and a consequent increase in ionic size [25]. Therefore, the decrease in TEC with Mn doping could be understood to be due to a decrease in the Co^{3+} content and a consequent suppression of both the spin state transitions and formation of oxygen vacancies as revealed by the TGA data in Fig. 3.

The temperature dependence of the electrical conductivity of the $Nd_{0.6}Sr_{0.4}Co_{1-y}Mn_yO_{3-\delta}$ samples is shown in Fig. 5. The decrease in conductivity observed at higher temperatures for the cobalt-rich compositions could be due to the formation of significant amount of oxide ion vacancies at higher temperatures as indicated by the TGA data (Fig. 3). The formation of oxide ion vacancies can cause a decrease in electrical conductivity due to a decrease in the charge carrier concentration and the perturbation of the periodic potential of the O–(Co,Mn)–O network.

At a given temperature, the electrical conductivity decreases with increasing Mn content similar to that found with Fe doping [18]. The $Nd_{0.6}Sr_{0.4}Co_{1-y}Mn_yO_{3-\delta}$ perovskite oxides are mixed hopping conductors with more than one type of transition metal ion and the charge compensation on replacing Nd^{3+} by Sr^{2+} can occur by the formation of Co^{4+} or Mn^{4+} or both. Tai et al. [26] and Kostogloudis et al. [27] have reported that the electronic charge compensation occurs preferentially by the formation of Fe^{4+} and Mn^{4+} rather than Co^{4+} in $La_{1-x}Sr_xCo_{1-y}Fe_yO_{3-\delta}$ and $Pr_{1-x}Sr_xCo_{1-y}Mn_yO_{3-\delta}$, respectively. This suggests that a preferential electronic charge compensation of $Mn^{3+} \rightarrow Mn^{4+}$ over that of $Co^{3+} \rightarrow Co^{4+}$ could also take place in the $Nd_{0.6}Sr_{0.4}Co_{1-y}Mn_yO_{3-\delta}$ system. Thus, the preferential formation of Mn^{4+} and an increase in the electron localization due to the decreased covalency of the Mn^{4+}–O bond compared to the Co^{4+}–O bond result in a decrease in the electrical conductivity with increasing Mn content.

The $Nd_{0.6}Sr_{0.4}Co_{1-y}Mn_yO_{3-\delta}$ system exhibits a metal to semiconductor transition around $y = 0.2$, which could be explained by considering the changes in the structural parameters as in the $Nd_{1-x}Sr_xCoO_{3-\delta}$ system described previously [14]. The end member $Nd_{0.6}Sr_{0.4}CoO_{3-\delta}$ is a metallic conductor with a large bandwidth and no charge transfer gap between the $Co^{3+/4+}$:3d and the top of the O^{2-}:2p bands. The substitution of a larger Mn^{3+} for Co^{3+} causes a decrease in the tolerance factor t and a bending of the O–(Co,Mn)–O bond (decrease in bond angle below 180°), which results in a decrease in the bandwidth. This together with a lying of the $Mn^{3+/4+}$:3d band above the $Co^{3+/4+}$:3d band leads to an opening of the charge transfer gap and a consequent metal to semiconductor transition.

The electrochemical performance of the cathode could be affected by the microstructure as well as the kinetics of oxygen exchange and diffusion. The BET surface area and the average crystallite size of the cathode powders do not vary significantly as listed in Table 1, and therefore influence of the geometrical morphology of the prepared powders on electrochemical performance could be neglected in this study. The firing temperature of the cathode–electrolyte assembly could

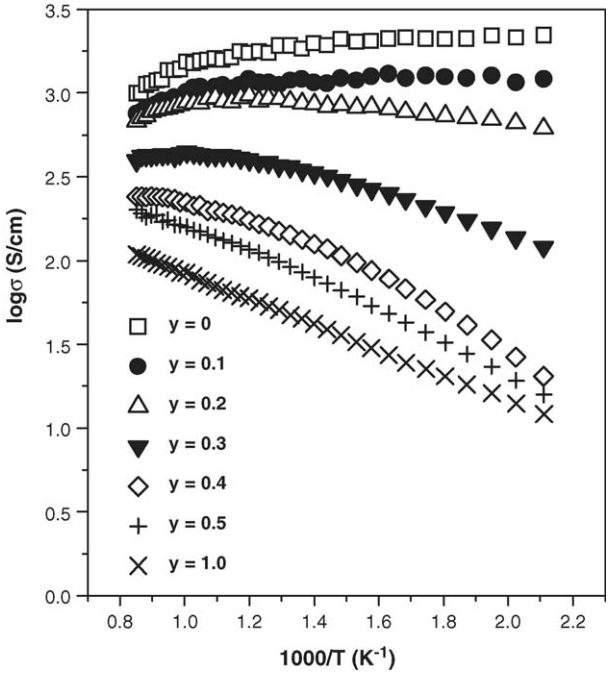

Fig. 5. Variations of the electrical conductivity measured in air of $Nd_{0.6}Sr_{0.4}Co_{1-y}Mn_yO_{3-\delta}$ with temperature for various values of y.

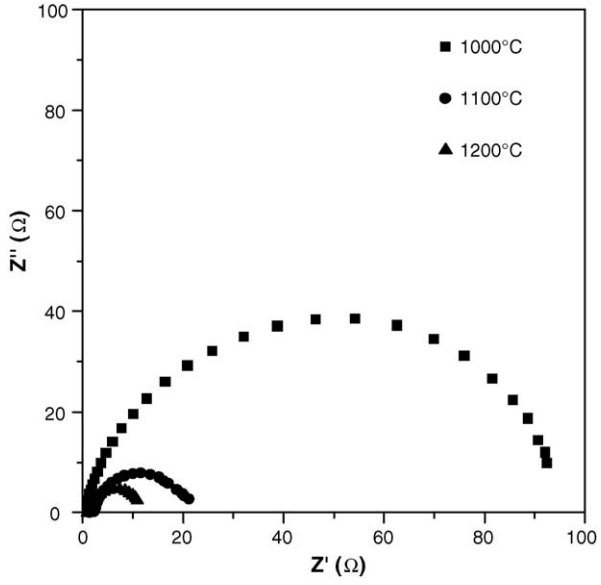

Fig. 6. AC impedance spectra recorded at 800 °C in air of the $Nd_{0.6}Sr_{0.4}Co_{0.8}Mn_{0.2}O_{3-\delta}$ cathode–LSGM electrolyte assembly after firing at various temperatures for 3 h.

also affect the interface, microstructure and the electrochemical performance. In order to optimize the interfacial and microstructural characteristics, AC impedance spectroscopic as well as SEM data were collected after firing the cathode–electrolyte assemblies at various temperatures. The AC impedance spectra of the $Nd_{0.6}Sr_{0.4}Co_{0.8}Mn_{0.2}O_{3-\delta}$ cathodes at 800 °C after firing at various temperatures for 3 h are shown in Fig. 6. The cathode–electrolyte assembly fired at 1000 °C shows a significantly high polarization resistance due to the poor interfacial contact at the low firing temperature. As seen in Fig. 7, the assembly fired at 1000 °C shows only point contacts between particles and poor adhesion between the cathode and electrolyte. On the other hand, the assemblies fired at 1100 and 1200 °C show area contact between particles and good adhesion between the cathode and electrolyte, which lead to low charge transfer resistance. Although the assembly fired at 1200 °C shows the lowest polarization resistance, it could not be considered as the optimum firing temperature due to the formation of new reaction products on firing the cathode–electrolyte mixture at 1200 °C (Fig. 8). Therefore, all cathode–electrolyte assemblies for single cell tests were fired at 1100 °C for 3 h.

The variations of the power density and the over-potential with current density at 800 °C for the various $Nd_{0.6}Sr_{0.4}Co_{1-y}Mn_yO_{3-\delta}$ cathode compositions are shown in Fig. 9. The power density decreases and the over-potential increases with increasing Mn content. Oxygen reduction at a porous cathode is limited not only by the charge transfer and the adsorption/dissociation of oxygen on cathode surface, but also by the transport of oxide ions through the cathode bulk and across the cathode/electrolyte interface. Therefore, cathode over-potential is closely related to the kinetics of oxygen exchange and diffusion in cathode materials as well as the electronic conductivity. Both the concentration of oxide ion vacancies and electrical conductivity decrease with increasing Mn

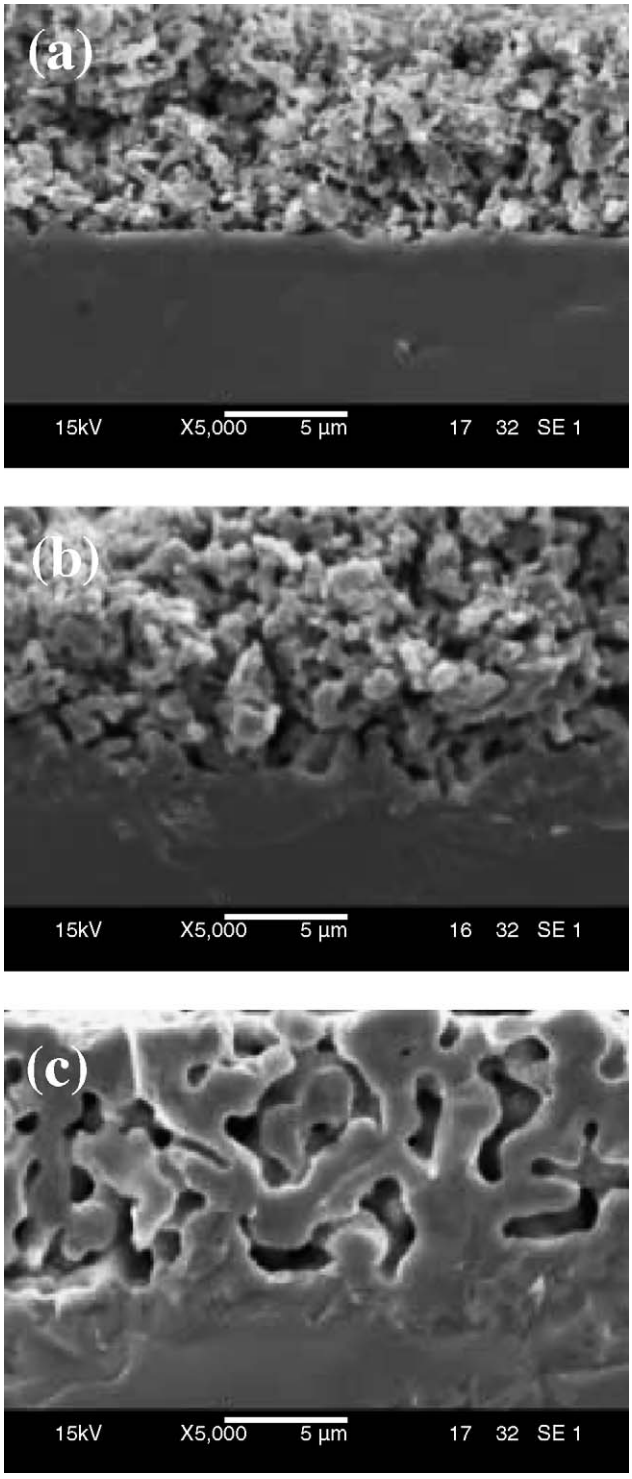

Fig. 7. SEM micrographs of the $Nd_{0.6}Sr_{0.4}Co_{0.8}Mn_{0.2}O_{3-\delta}$ cathode–LSGM electrolyte assembly after firing at (a) 1000 °C, (b) 1100 °C and (c) 1200 °C for 3 h.

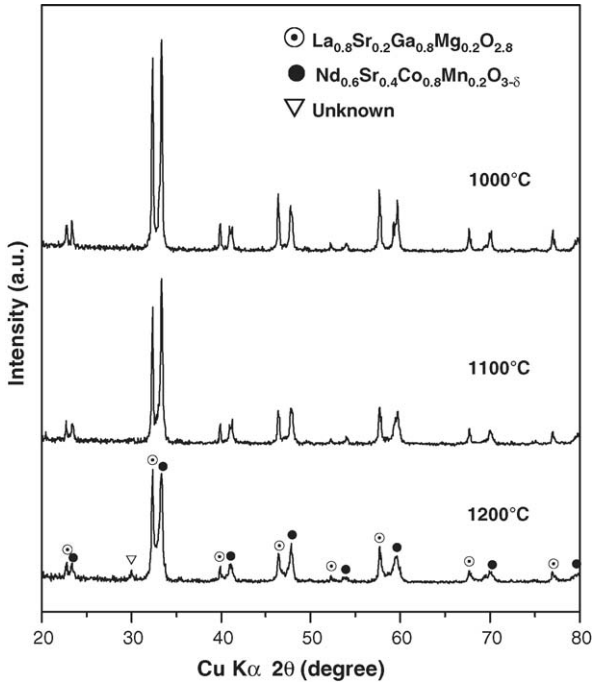

Fig. 8. X-ray powder diffraction patterns recorded after heating the $Nd_{0.6}Sr_{0.4}Co_{0.8}Mn_{0.2}O_{3-\delta}$ cathode and the LSGM electrolyte powders at various temperatures for 3 h.

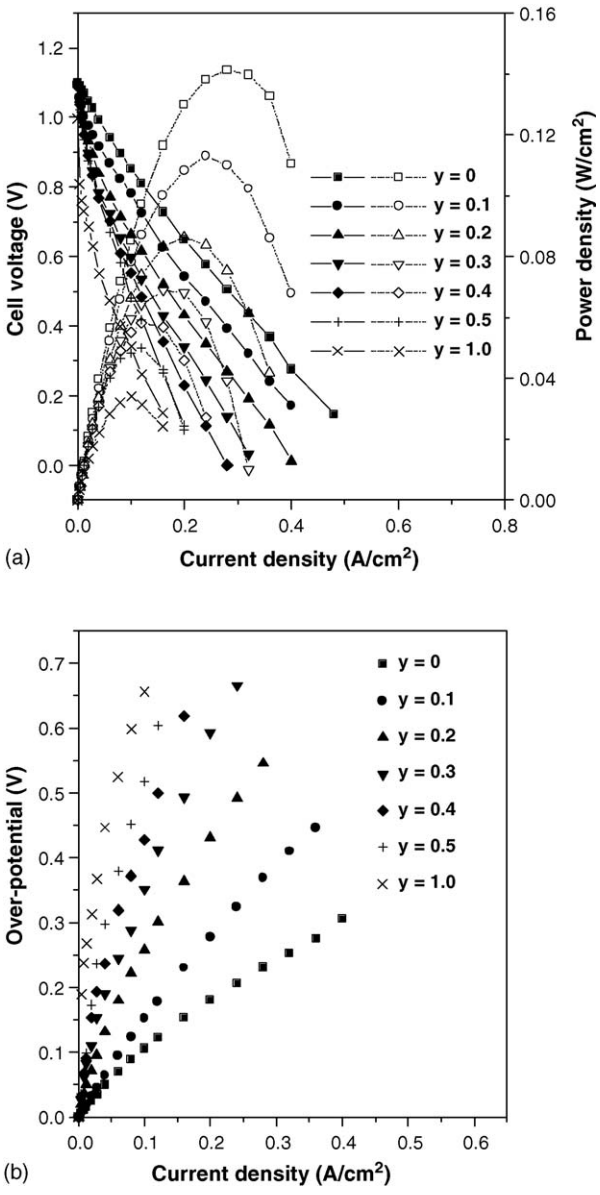

Fig. 9. Electrochemical performance data of the $Nd_{0.6}Sr_{0.4}Co_{1-y}Mn_yO_{3-\delta}$/LSGM/Ni–GDC single cells at 800 °C: variations of (a) the *I–V* curve (closed symbols) and power density (open symbols) and (b) cathode over-potential.

doping as evident from the data in Figs. 3 and 5. Gao et al. [28] have reported that high oxide ion vacancy concentration in the surface of the cathode could improve the dissociation of oxygen molecule O_2(ad) into atomic oxygen O_{ad}. It has also been reported that the oxygen self-diffusion coefficients in the manganates are several orders of magnitude lower than those in the cobaltates and the activation energies for oxygen self-diffusion are considerably higher in the manganates compared to that in the cobaltates [29]. Thus, the decreasing oxide ion vacancy concentration and electrical conductivity with Mn doping appear to decrease the oxygen exchange and the transport speed of oxide ions as well as the charge transfer, leading to a decrease in the electrochemical performance.

4. Conclusions

The $Nd_{0.6}Sr_{0.4}Co_{1-y}Mn_yO_{3-\delta}$ ($0 \le y \le 1.0$) system has been investigated as a cathode material for intermediate temperature SOFC by characterizing its crystal chemistry, thermal expansion, oxygen loss behavior, electrical conductivity and electrocatalytic activity. Although the thermal expansion decreases favorably with Mn doping, the electrocatalytic activity also decreases due to a decrease in the oxygen vacancy concentration and electrical conductivity; the system exhibits a metal to semiconductor transition around $y = 0.2$. Thus, a trade-off between electrochemical performance and thermal expansion may be necessary to identify optimum cathode compositions for intermediate temperature SOFC.

Acknowledgement

This work was supported by the Welch Foundation Grant F-1254.

References

[1] N.Q. Minh, J. Am. Ceram. Soc. 76 (1993) 563.
[2] T. Tsai, S.A. Barnett, Solid State Ionics 93 (1997) 207.
[3] M.T. Colomer, B.C.H. Steele, J.A. Kilner, Solid State Ionics 147 (2002) 41.
[4] S.B. Adler, Solid State Ionics 111 (1998) 125.
[5] A.N. Petrov, O.F. Kononchuk, A.V. Andreev, V.A. Cherepano, P. Kofstad, Solid State Ionics 80 (1995) 189.
[6] T. Kawada, J. Suzuki, M. Sase, A. Kaimai, K. Yashiro, Y. Nigara, J. Mizusaki, K. Kawamura, H. Yugami, J. Electrochem. Soc. 149 (2002) E252.
[7] M. Mori, Y. Hiei, N. Sammes, G.A. Tompsett, J. Electrochem. Soc. 147 (2000) 1295.
[8] Y. Takeda, H. Ueno, N. Imanishi, O. Yamamoto, N. Sammes, M.B. Phillipps, Solid State Ionics 86–88 (1996) 1187.
[9] M. Koyama, C. Wen, T. Masuyama, J. Otomo, H. Fukunaga, K. Yamade, K. Eguchi, H. Takahashi, J. Electrochem. Soc. 148 (2001) A795.
[10] G.Ch. Kostogloudis, N. Vasilakos, Ch. Ftikos, Solid State Ionics 106 (1998) 207.
[11] H.Y. Tu, Y. Takeda, N. Imanishi, O. Yamamoto, Solid State Ionics 100 (1997) 283.
[12] P. Shuk, V. Charton, V. Samochval, Mater. Sci. Forum 76 (1991) 161.
[13] C.H. Yo, K.S. Roh, S.J. Lee, K.H. Kim, E.J. Oh, J. Korean Chem. Soc. 35 (1991) 211.
[14] K.T. Lee, A. Manthiram, J. Electrochem. Soc. 152 (2005) A197.
[15] L.A. Chick, L.R. Pedersen, G.D. Maupin, J.L. Bates, L.E. Thomas, G.J. Exarhos, Mater. Lett. 10 (1990) 6.
[16] R.D. Shannon, Acta Crystallogr. A32 (1976) 751.
[17] M.B. Phillipps, N.M. Sammes, O. Yamamoto, Solid State Ionics 123 (1999) 131.
[18] K.T. Lee, A. Manthiram, Solid State Ionics 176 (2005) 1521.
[19] B.C.H. Steele, Mater. Sci. Eng. B13 (1992) 79.
[20] J. Mizusaki, H. Tagawa, K. Naraya, T. Sasamoto, Solid State Ionics 49 (1991) 111.
[21] J. Mizusaki, Y. Mima, S. Yamauchi, H. Tagawa, J. Solid State Chem. 80 (1989) 102.
[22] N. Dasgupta, R. Krishnamoorthy, K.T. Jacob, Solid State Ionics 149 (2002) 227.
[23] S.V. Chavan, S.J. Patwe, A.K. Tyagi, J. Alloy. Compd. 360 (2003) 189.

[24] K. Huang, H.Y. Lee, J.B. Goodenough, J. Electrochem. Soc. 145 (1998) 3220.
[25] H. Hayashi, M. Kanoh, C.J. Quan, H. Inaba, S. Wang, M. Dokiya, H. Tagawa, Solid State Ionics 132 (2000) 227.
[26] L.W. Tai, M.M. Nasrallah, H.U. Anderson, D.M. Sparlin, S.R. Sehlin, Solid State Ionics 76 (1995) 259.
[27] G.Ch. Kostogloudis, P. Fertis, Ch. Ftikos, Solid State Ionics 118 (1999) 241.
[28] J. Gao, X. Liu, D. Peng, G. Meng, Catal. Today 82 (2003) 207.
[29] S. Carter, A. Selcuk, R.J. Chater, J. Kajda, J.A. Kilner, B.C.H. Steele, Solid State Ionics 53–56 (1992) 597.